Pergamon

Journal of Structural Geology, Vol. 18, No. 1, pp. 75 to 91, 1996

0191-8141/96 $15.00 + 0.00

0191-8141(95)00084-4

The pyrite-type strain fringes from Lourdes (France): indicators of Alpine thrust kinematics in the Pyrenees

DOMINGO G. A. M. AERDEN

Laboratoire de Géophysique et Tectonique (URA-CNRS 1760), case courrier 060, Université de Montpellier II, 34095 Montpellier, France

(*Received* 19 *January* 1995; *accepted in revised form* 19 *July* 1995)

Abstract—A new method is developed to reconstruct polyphase deformation histories from pyrite grains with displacement-controlled fibrous strain fringes. It decomposes the relative displacement between a pyrite grain and a fringe into incremental rotations and pull-apart directions. Application to a classic specimen from Lourdes (France) shows that the rotations determine the fibre curvature sense, and strongly depend on local strain parameters as well as the initial orientation and shape of pyrite grains. In contrast, pull-apart directions appear to be relatively constant and straight, although curved pull-apart trajectories were expected from the heterogeneous, non-coaxial deformation in the matrix. The discrepancy is due to the localization of shear-strain components around pyrite-fringe complexes. The complexes themselves represent ellipsoidal domains of relatively coaxial strain that parallel a regional crenulation cleavage, even in zones lacking this cleavage due to stretching and shearing of a pre-existing foliation (S_1). Thus, strain fringes consistently record bulk shortening orientations regardless of local variations in strain parameters and microstructural development. The analysed pyrite-fringe complexes from Lourdes were previously considered as classic shear-sense indicators, but yield hook-shaped pull-apart trajectories in the new method. This indicates two deformation events that can be related to a sub-horizontal (S_2) and steep regional crenulation-cleavage (S_3). The recorded polyphase deformation history is tentatively interpreted in terms of a change from gravitational spreading to a compressive emplacement of a thrust sheet in the North Pyrenean foreland.

INTRODUCTION

Strain fringes are syntectonic mineral aggregates that develop at dilatant margins between a rigid body and the deforming matrix (Mügge 1930, Pabst 1931). They have been previously termed 'pressure shadow' (Pabst 1931) or 'pressure fringe' (Spry 1969) but 'strain fringe' (Passchier & Trouw 1995) seems the best designation as the microstructure results not from pressure but from strain. It is also a better distinction from 'strain *shadow*' (a low-strain domain adjacent to a competent body). Strain fringes are not to be confused either with 'wings' or 'tails' of porphyroclasts, which form by entrainment of deformed porphyroclast material along the foliation.

Due to anisotropic growth kinetics, strain fringes commonly develop a fibrous internal structure, which records the displacement between the rigid object and the growing fringes. This quality makes them unique kinematic indicators. The main problem, however, is that the recorded (relative) motion between fringes and object has to be translated in terms of matrix strain and reoriented in the regional tectonic framework. Several models have been proposed and applied in mechanical studies of various geological structures, such as folds, nappes and accretionary prisms (Zwart & Oele 1966, Spry 1969, Durney & Ramsay 1973, Beutner & Diegel 1985, Wickham 1973, Ramsay & Huber 1983, Ellis 1986, Choukroune 1971, 1976, Etchecopar & Malavieille 1987, Dietrich 1989, Gray & Willman 1991, Fischer & Byrne 1992, Fisher & Anastasio 1994; Kirkwood *et al.* 1995).

Different assumptions of these authors concerning the rotation of rigid grains during non-coaxial deformation have led to conflicting interpretations, even concerning the shear sense indicated by a given strain fringe asymmetry. Most authors assume that curved fibres record progressive changes in the incremental pull-apart direction between the fringes and the rigid grains. In the X–Z plane of a non-coaxial deformation, this would correspond to the progressive rotation of the cumulative strain ellipse in the matrix (Beutner & Diegel 1985). Thus, fibres that curve clockwise in the growth direction would indicate a dextral shear sense (Fig. 1a). This concept requires, however, that neither the rigid grain nor the fringes rotate relative to the plane of shearing and do not influence the fibre pattern in this way. This is a point of general disagreement. Zwart & Oele (1966) and Spry (1969) considered that rigid objects do rotate, but treated the strain fringes as non-rotating. Ellis (1986), conversly, considered that only spherical pyrite

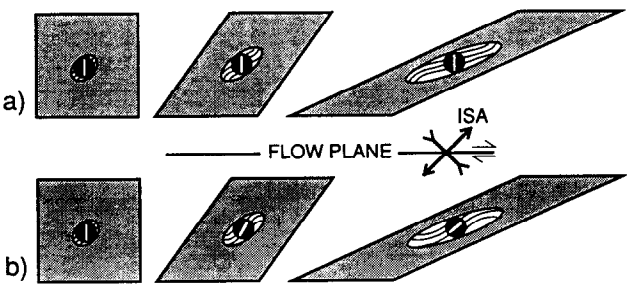

Fig. 1. End-member interpretations for the development of asymmetric strain fringes in the X–Z plane of a non-coaxial deformation. (a) The object is not permitted to rotate and fibres track the rotation of the accumulative strain ellipse in the matrix. (b) Fibre curvature is now determined by rotation of the rigid object, induced by shearing in the matrix. No direct relationship exists between fibre directions and principal strain axes.

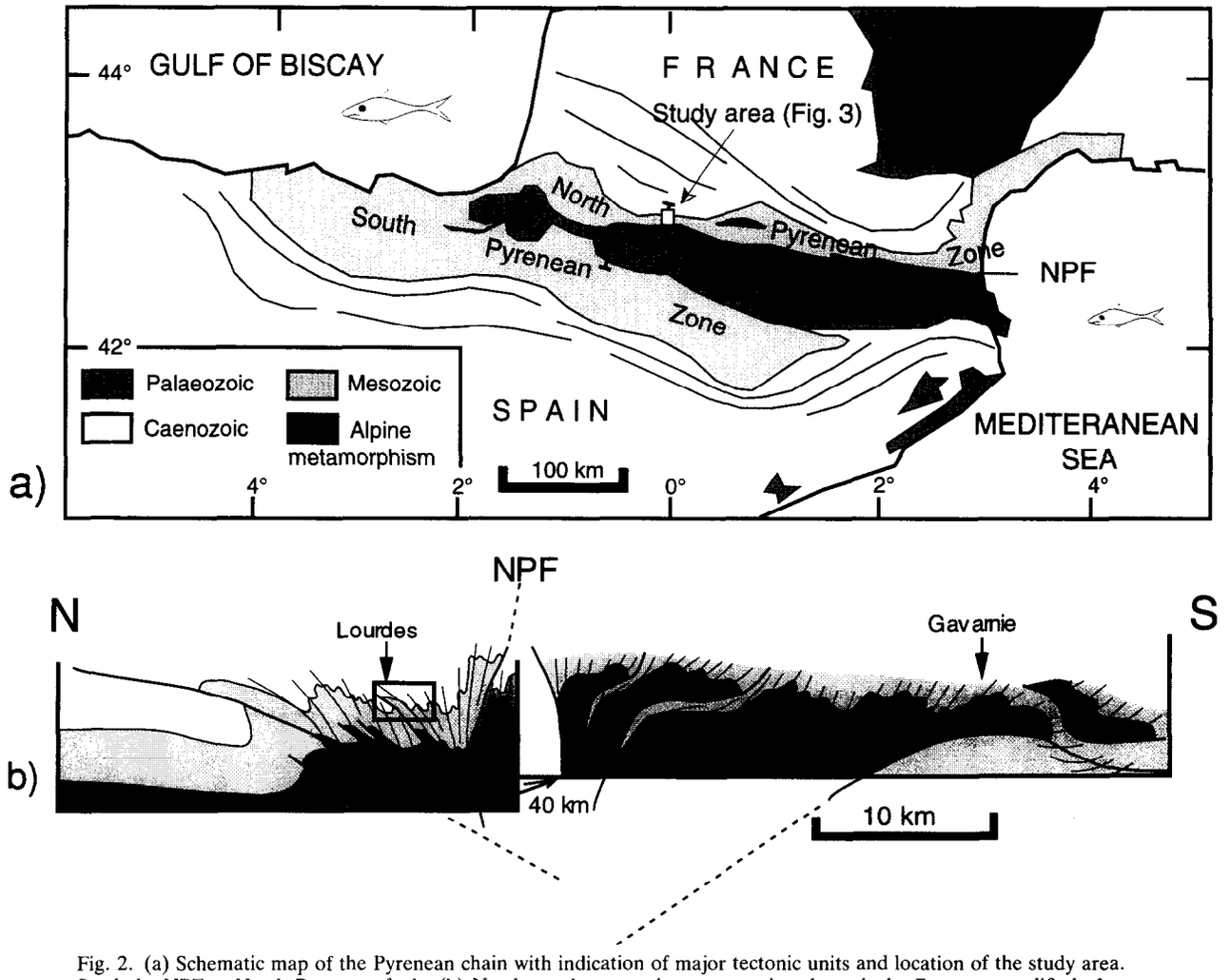

Fig. 2. (a) Schematic map of the Pyrenean chain with indication of major tectonic units and location of the study area. Symbols: NPF = North Pyrenean fault. (b) North–south composite cross-section through the Pyrenees modified after Choukroune (1976), showing the attitude of the main foliation (S_1) and location of major thrusts. Stippled lines confine the orogen between the Iberian and European plate.

grains do not rotate but that the strain fringes do. Choukroune (1971, 1976) and Etchecopar & Malavieille (1987) considered that rigid objects and their strain fringes both rotate and, consequently, from a given fringe asymmetry, they conclude the opposite shear sense than the other authors.

This study attempts to clarify some of the above uncertainties and to improve our understanding of strain fringe kinematics as a function of matrix deformation. It combines microstructural analyses and computer simulation of superb pyrite-fringe complexes from a classic location near Lourdes, and considers this within the regional tectonic context. The analysed fringes preserve pristine fibrous structures and the pyrite grains have variable geometries, allowing for study of the influence of shape-induced rotations. A new method is developed that decomposes the relative movement between a pyrite grain and its strain fringes into rotation and translation components and then re-orients these in the regional tectonic framework. The method enables one to distinguish single from polyphase deformation paths. In fact, one of the main conclusions is that the asymmetric strain fringes from Lourdes, which are textbook shear-sense indicators (Hanner & Passchier 1991, Passchier & Trouw 1995), actually record two distinct deformation events. Implications for the dynamics of a foreland thrust sequence hosting these microstructures will be discussed.

TECTONIC SETTING

The Pyrenees form part of the Alpine fold belt in Europe and resulted from the collision between the Iberian and European plates during Upper Cretaceous–Eocene times (Choukroune & Mattauer 1978). It is not certain if a subduction zone fully developed or not. The belt has been subdivided into southern and northern zones, in which mainly Mesozoic and Tertiary sediments are exposed separated by a core zone of Paleozoic basement (the 'axial zone'; Fig. 2a). Palaeozoic basement is also exposed in the North Pyrenean zone as a number of isolated massifs brought up as fault-bounded blocks. The boundary between the axial zone and the North Pyrenean zone is a lithospheric transpression zone known as the 'North Pyrenean fault zone', along which a 400 km of sinistral strike-slip has been inferred (Choukroune 1976, Choukroune & Mattauer 1978).

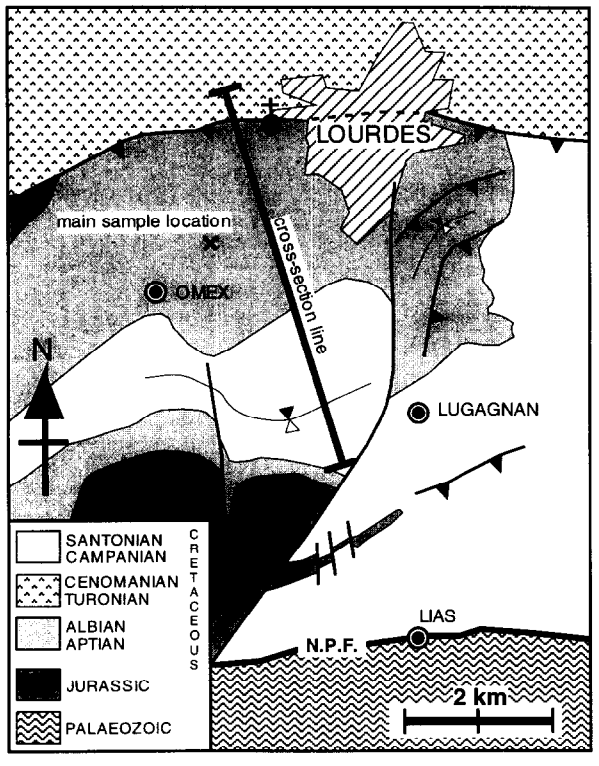

Fig. 3. Simplified geological map of the study area after the 1:50 000 B.R.G.M. geological map and Choukroune (1969).

This zone is associated with a narrow belt of greenschist grade metamorphosed Mesozoic rocks and a number of small peridotite occurrences, notably near Lherz (lherzolites). External folds and thrusts verge opposite on either side of the orogen giving it a high degree of symmetry (Fig. 2b). The regionally dominant cleavage and main folds belong to a first deformation phase, but a polyphase deformation history is recorded by the presence of pervasive crenulation cleavages (Choukroune *et al.* 1980). This study provides insight into their tectonic significance, which has remained unclarified to date.

STRUCTURAL ANALYSIS

The main foliation (S_1) is axial plane to the regional scale folds and describes half a fan between the North Pyrenean fault zone, where it is sub-vertical, and a basal thrust further north where it dips gently south (Choukroune 1969; Figs. 3 and 4). In the proximity of a major thrust at Lourdes, reverse shear along this foliation is indicated by a down-dip stretching lineation, the asymmetry of sigmoidal veins and the offsets of veinlets across cleavage lamellae. Thin S_1 parallel calcite veinlets are strongly boudinaged in both north–south and east–west directions (Fig. 4a), recording an oblate finite strain geometry ($K < 1$). As the boudins have rectangular shapes and appear little deformed, their added lengths (l_0) compared to the distance they span (l) provides a minimum approximation of the amount of elongation ($l - l_0/l_0$). Values of 140% in east–west sections and 180% in north–south sections were obtained in this manner.

Three (younger) crenulation cleavages were recognized (S_2–S_4) whose tectonic significance will be interpreted together with results from strain-fringe analysis later. The main crenulation cleavage (S_3) dips moderately–steeply south and is associated with up to decametric scale F_3 folds (Fig. 4). Where intensely developed, S_3 is macroscopically indistinguishable from S_1. It is selectively developed in short limbs of F_3 folds and disappears gradually downwards towards the thrust plane. However, the highly sheared rocks near the thrust do preserve relics of S_3 within relatively quartz-rich, low-strain pods and in the strain shadows of pyrite-fringe complexes (Figs. 4e, 5a–c, 6a&b, and 7a–d). The transition of low-strain domains to the strongly sheared matrix shows a progressive straightening out or 'de-crenulation' of the main foliation (S_1) as the angle with S_3 decreases. Thus, crenulations progressively open up until they disappear completely and a sheared S_1 remains (Figs. 5b&c and 6b). The distribution of S_3 at different scales reflects a heterogeneous orientation of S_1 in the D_3 deformation field as interpreted in Fig. 5d. S_1 has a shortening orientation in domains of relatively coaxial, low strain (preserving crenulation) and an extensional orientation in domains of high, non-coaxial strain. Here crenulations are not developed, due to stretching of S_1. Local zones with isoclinal crenulation or 'transposition' of S_1 may be regarded as zones of high, but relatively coaxial, strain.

Relics of an older crenulation cleavage (S_2) are preserved inside S_3 microlithons (Fig. 4g) and in strain shadows (Figs. 5a, 6c and 7a–d), but no macroscopic F_2 folds have been identified. A younger, sub-horizontal crenulation cleavage (S_4) is weakly developed in the southern part of the area (Fig. 4d).

PYRITE STRAIN FRINGE COMPLEXES

Kinematics of fibre growth in strain fringes

Strain fringes have been classified as antitaxial or syntaxial to designate growth at the internal object–fringe or the external fringe–matrix contact, respectively (Durney & Ramsay 1973, Ramsay & Huber 1983). Note that this is somewhat misleading with respect to the inverse classification by the same authors of fibrous veins (syntaxial for growth at the vein centre; antitaxial for growth at the vein–matrix contact). Antitaxial fringe growth is favoured when the object–matrix boundary is less coherent than the fringe–matrix boundary, because of low crystallographic affinity with the matrix minerals. This is generally the case for pyrite grains with silicate strain fringes in a siliceous matrix. Strain fringes can be further classified according to whether they behaved rigidly or deformed. Finally, antitaxial fibres may grow perpendicular to crystal faces of the rigid object (face-controlled fibres), or may track the displacement between once adjacent points (displacement-controlled fibres). Face-controlled fibre growth is promoted by smooth, flat crystal faces such as euhedral pyrite. It is

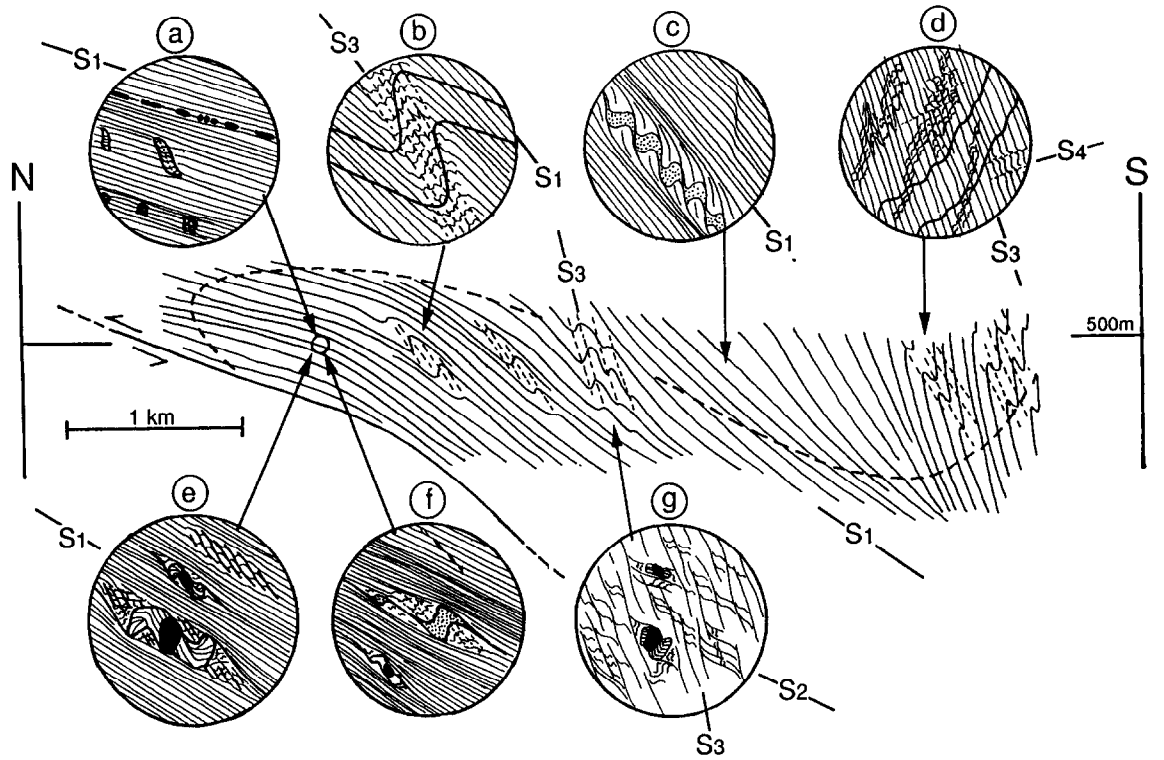

Fig. 4. Composite structural cross-section in the study area showing foliation attitudes and the relationships with some characteristic small-scale structures. The approximate regional attitude of bedding is indicated with the heavy dashed line. Insets show: (a) boudinage of the foliation and of carbonate veins (black), indicating a north–south elongated, pancake-shaped finite strain ellipsoid. (b) S_3 is preferentially present in short limbs of F_3 folds, in which strain is inferred to be lower. (c) Vertical strain partitioning surfaces cutting a quartz vein are interpreted as a coarsely spaced S_3. In the surrounding rock, the D_3 deformation mechanism is inferred to be S_1-induced shearing. Compare with (f). (d) The S_1/S_2 fabric is microscopically visible and a weak flat crenulation cleavage is developed (S_4). (e) The fringe-pyrite complexes analysed in this paper, S_2 and S_3 are preserved in strain shadows of the complexes and in low-strain matrix pods. (f) similar structure to (c), but with a greater component of shearing; S_3 is preserved in the strain shadows of disrupted vein segments, but destroyed elsewhere due to S_1–parallel shearing. Note reverse offset of thin veinlets by S_1. (g) Pyrite grains recording D_2 and D_3 parallel extension in fibres.

uncertain whether fibres in strain fringes grew continuously (cf. Dietrich 1989) or in an incremental 'crack–seal' fashion (Ramsay 1980). The lack of inclusion bands (typical crack–seal features in veins) is inconclusive, as growth at the pyrite interface would have precluded formation of inclusion bands by syntaxial overgrowth of wallrock micas. However, the question is not relevant to the kinematic analysis in this paper.

Description of the examples from Lourdes

The strain figures analysed here show the typical features of rigid, antitaxial, displacement-controlled fibres (the 'pyrite type' of Ramsay & Huber 1983), which seems to be the most common type in nature. That is, they preserve a pristine internal structure of parallel fibres with few recrystallization features, fibre curvature is not associated with bent crystal lattices (no sweeping extinction of fibres) and distal fringe boundaries are not tapered, but reflect the pyrite shape. They were mainly collected from lower Cretaceous (Aptian) slates, approximately 2 km south of the famous Roman Catholic sanctuary at Lourdes, in the immediate hangingwall of a thrust (Fig. 3). The pyrite grains vary in size between 1 and 5 mm, have irregular outlines and variable elongation ratio. All pyrite-fringe complexes have asymmetric strain fringes containing curved fibres with one or multiple internal truncation surfaces. At their distal ends, the complexes are generally bound by conspicuous carbon- and mica-enriched, high-strain zones with consistent asymmetric disposition about the pyrite-fringe complexes and oblique to the main foliation (Figs. 5b, 6a and 7a–d). These zones are sub-parallel to relic S_3 in strain shadows and are inferred to have formed by intensification of D_3 strain against the rigid fringe edges. Minor dissolution of fringe edges is occasionally suggested.

Due to their rigid behaviour, pyrite-fringe complexes are associated with four strain-protected zones or 'strain shadows': two at their extremities and two within the hinge regions. These contain relics of two crenulation cleavages (S_2 and S_3), the latter of which exhibits the described progressive decrenulation towards the sheared matrix (Figs. 5, 6 and 7). The same is observed in strain gradients associated with competent quartz veins, psammitic beds and in low-strain matrix pods. Most pyrite grains contain aligned mica inclusions or cleaved matrix fragments, indicating overgrowth of S_1 and an origin of pyrite, probably as early syn-D_2 metamorphic porphyroblasts. The orientation of these inclusion trails varies from pyrite to pyrite grain, suggesting differential rotations. Strain fringes are exclusively developed in

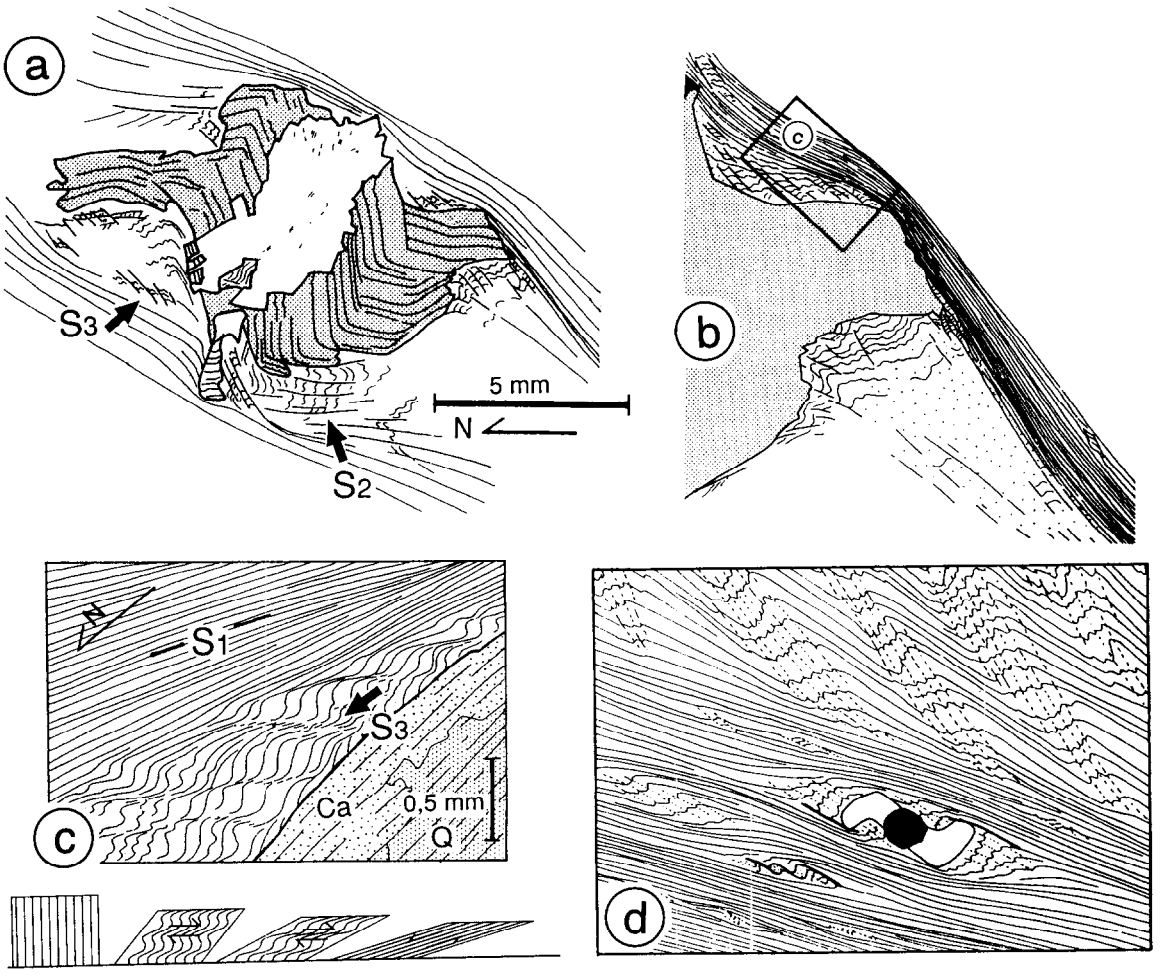

Fig. 5. (a) Pyrite-fringe complex with strongly hooked fibre patterns, high angle internal truncation surfaces and relics of two crenulation cleavages in strain-protected zones, which correlate with fibre directions. (b) Detailed view of the right hand side of (a), showing the relationships between relic S_3 and the dominant matrix foliation (S_1). (c) Further magnified view of the area indicated in (b), showing progressive decrenulation of S_1 towards the sheared matrix. The transition is inferred to represent different kinematic stages of D_3 deformation as schematically drawn below the figure. (d) Interpretation of the distribution of S_3 and S_1 in a strongly heterogeneous strain field; S_3 is absent where S_1 is oriented in the extensional field of the D_3 deformation, i.e. in long limbs of F_3 folds and towards the thrust plane. High-strain caps (or shear bands) at the distal ends of pyrite-fringe complexes represent D_3 strain intensifications that locally truncate S_1. The figure is not to scale.

north–south vertical planes, which seems to imply that the 140% shortening recorded by boudinaged veinlets in an east–west direction (see above) accumulated earlier, during D_1. Thus, the strain fringes developed in the X–Z plane of deformation, probably under plane strain conditions. However, we cannot completely exclude that the east–west strain accumulated partially during strain fringe growth strain-rate dependent deviatoric stresses if stayed below some critical value for pyrite-matrix decoupling in this direction to occur.

STRAIN FRINGE GROWTH AS A FUNCTION OF MATRIX DEFORMATION

Rigid pyrite-fringe complexes can be regarded as three fragments that are progressively pulled apart from each other during deformation. In this concept, the finite geometry of displacement-controlled fibres will be determined by two counteracting components of movement. (i) The relative translation (or pull-apart direction) between a rigid object and its accumulated fringe stages. This will initially be parallel to the instantaneous stretching axis (i.e. inclined at 45° to the flow plane for simple shear), but as the object–fringe complex gradually becomes elongate, the direction in which the three fragments are pulled apart will progressively rotate towards the flow-plane. For a dextral shear sense this '*translation component*' will tend to produce strain fringes with a 'Z' asymmetry and a maximum of 45° fibre curvature (Fig. 1a). (ii) Rigid objects and their strain fringes may undergo shape- or shearing-induced rotations about axes located near their geometric centres. These obviously depend on the shape and initial orientation of the rigid object. The fibre curvature resulting from this 'rotation component' is opposite to that produced by the above '*translation component*' (Fig. 1b). Note that a coaxial deformation can produce asymmetric curved fibres purely due to this rotation component (Fig. 8a).

Above, we have considered the ideal case of homogeneous progressive deformations, but more complex

fringe geometries can be expected from changes in deformation parameters with time. Three situations are envisaged for natural rock deformation.

(1) Changes in vorticity of a deformation with constant shearing plane, either due to external changes in boundary conditions or internal shifts in the patterns of shear-strain distribution.

(2) Polyphase deformation, involving a superposition of different deformation regimes and different incremental extension directions around pyrite grains (Fig. 8b; Choukroune 1971, Spencer 1991, Fischer & Byrne 1992).

(3) Changes in local shearing and extension directions due to a re-partitioning of deformation controlled by rock anisotropy (Fig. 8c). For example, a pre-existing foliation or bedding may first rotate and deform passively but start controlling the internal partitioning of deformation later (Bell 1986, Aerden 1985) and change the local extension direction around rigid grains (Fig. 8c; Wickham & Anthony 1977).

These deformation histories can produce closely resembling fringe morphologies and any method to analyse pyrite-fringe complexes must therefore be coupled to a careful analysis of deformation in the matrix as well as on regional scale.

STRAIN FRINGE ANALYSIS

Method

Six pyrite-fringe complexes representing the full range of morphologies encountered were analysed in detail (Figs. 9a–f). For each pyrite grain, a series of incremental translations and rotations were performed to most faithfully reproduce the natural fibre pattern, assuming ideal displacement-controlled fibre growth. This reconstruction was aided by a simple computer graphics programme (Adobe Illustrator 3.2) which allowed (i) superposition of the reconstructed figure on a scanned image of the natural fibre pattern and (ii) rotation of geometric figures about selected points. The method consists of incrementally retracing a marginal point on the pyrite grain along the fibre that departs at that point. This point is fixed at regular intervals on the fibre and the pyrite grain rotated about it each time until all other marginal points move closest to their corresponding fibres. The centre of the pyrite grain is plotted for each movement increment to show the relative translation between the pyrite grain and the accumulated fringe stages (Fig. 10).

After this exercise, the fibre development predicted from this modelling is obtained by connecting corresponding marginal points between the incremental displacement stages. The external fringe boundary is copied directly from the natural specimen. Each movement stage is then drawn separately (Fig. 11) to graphically show the predicted kinematics of fringe growth. A strong correspondence between natural and modelled fibre patterns is immediately apparent (compare Figs. 9 and 11) and confirms that fibres grew approximately 'displacement-controlled'. The absolute orientations of different fringe stages in Fig. 11 (relative to horizontal) is based on assumptions discussed in a later section.

Results and comparison with numerical models

Although the kinkiness vs roundness of the obtained pyrite centre trajectories (PCTs) is variable, they are consistently hook-shaped, recording an abrupt change in pull-apart directions of up to 90° (Fig. 10). This finding conflicts with the theoretically predicted maximum of 45° curvature (for progressive simple shear), also obtained in previous computer simulations after natural specimen from the Lourdes area (Etchecopar & Malavieille 1987). I have applied the same simulation method to the newly collected specimen with essentially the same result (Fig. 12).

Thus, there is a disagreement between, on the one hand, theoretical and computer-generated PCTs, which curve smoothly and moderately and, on the other hand, the PCTs reconstructed by the present method, which reveals sharp directional changes in PCTs and angle of up to 90°. A number of other discrepancies between computer simulation and natural examples are apparent. Firstly, internal fibre truncations show angles of up to 80° in the natural fringes but are absent or very small (less than 5°) in the computed models. Secondly, computed fibres are generally 'open' at both ends (Fig. 12), whereas this is not seen in the natural examples. Thirdly, natural fibres may curve up to 150° (Fig. 9e) but never curve more than 90° in the simulation. Finally, the last displacement increments in the reconstructed PCTs (most proximal to the pyrite grains) are strongly oblique to the matrix foliation, whereas they are sub-parallel in the calculated models. As will be shown and discussed below, these discrepancies are due to a two-phase deformation history and to deformation–partitioning effects around the rigid pyrite-fringe complexes.

Interpretation

The sharp bends in PCTs indicate an abrupt change in instantaneous stretching direction around pyrite grains

Fig. 6. (a) Photograph of a large thin section with pyrite-fringe complexes from the main sampling site. Note slightly darker strain differentiation bands (S_3) developed against the extremities of each complex, oblique to the main foliation. A detailed microstructural sketch of the complex most to the right is given in Fig. 5(a). (b) Microphotograph of the strain-protected zone indicated in (a) preserving F_3 crenulations. A line diagram of the boxed area is given in Fig. 5(c). (c) Microphotograph of the strain-protected zone indicated in (a), preserving F_2 crenulations. (d) Pyrite grain of Fig. 9(b), whose strain fringes show a sharp change in fibre direction, associated with a high angle internal truncation surface. This is difficult to explain in terms of progressive shearing deformation.

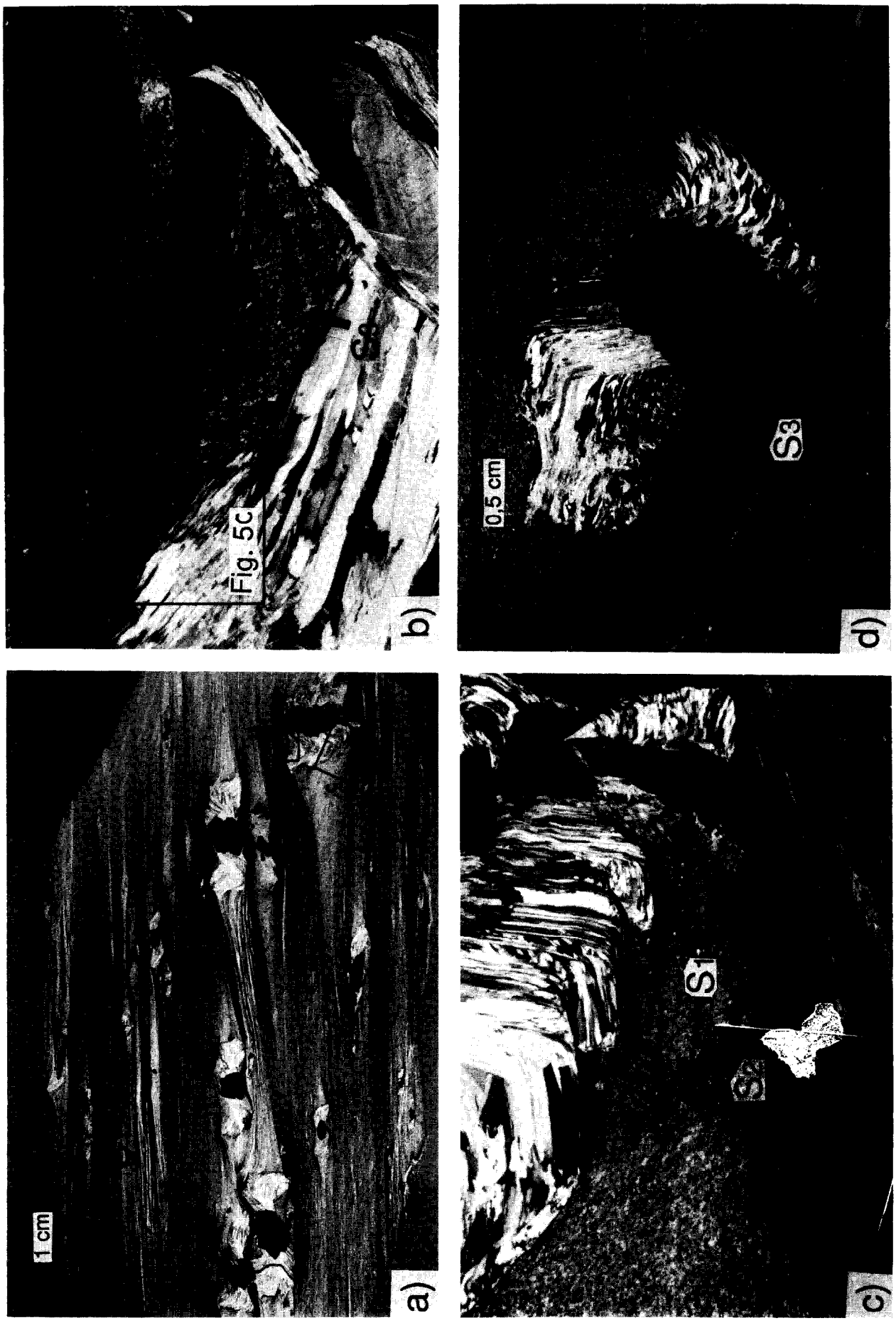

Fig. 6.

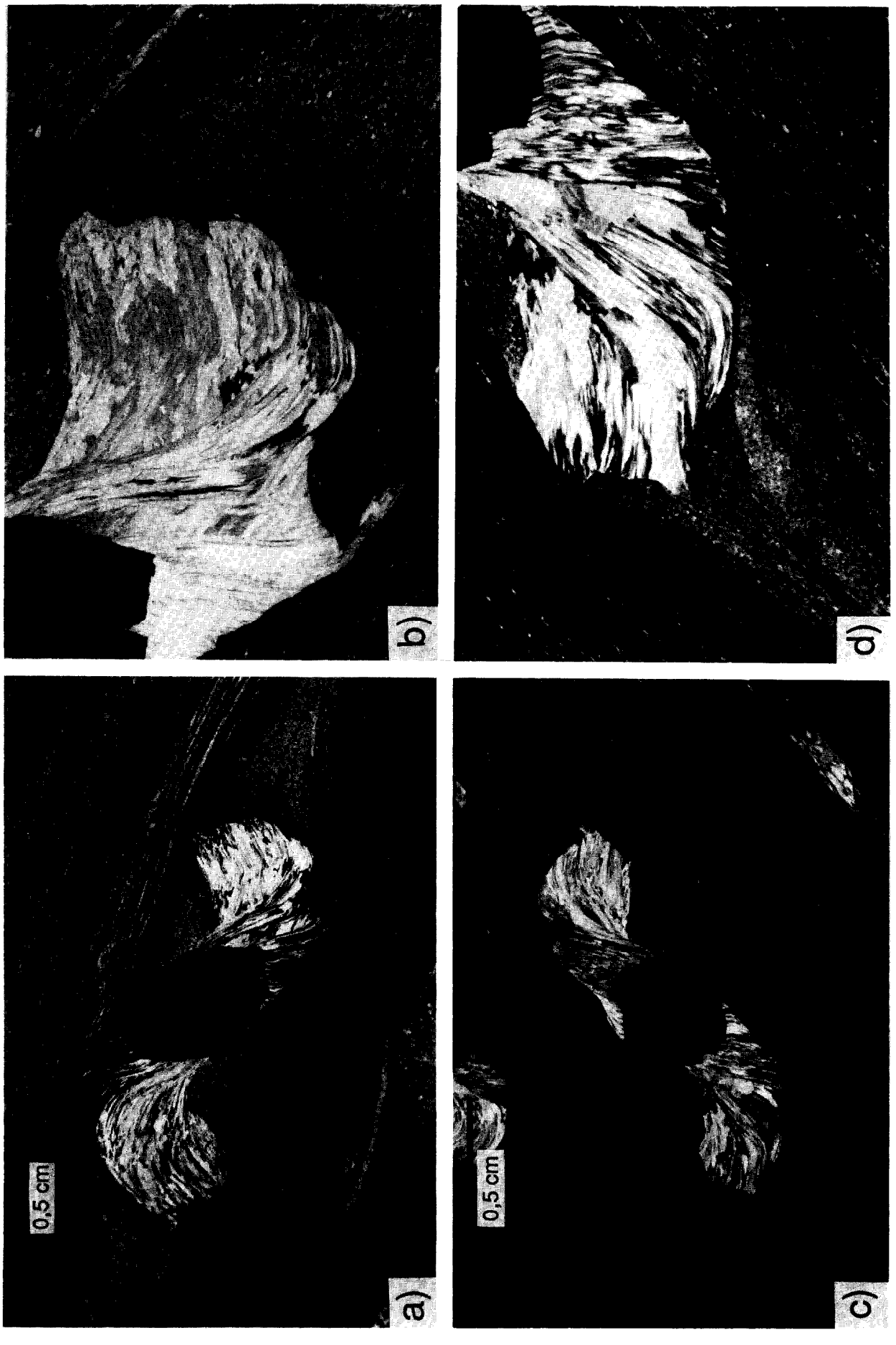

Fig. 7. (a) Microphotograph of the pyrite-fringe complexes with progressive fibre curvature. See line diagrams of Figs. 9(a), 10(a) and 11(a). (b) Detail of (a). Note the presence of S_2 and S_3. (c) & (d) A second example of what is shown in (a) and (b), respectively, but this thin section faces in the opposite direction.

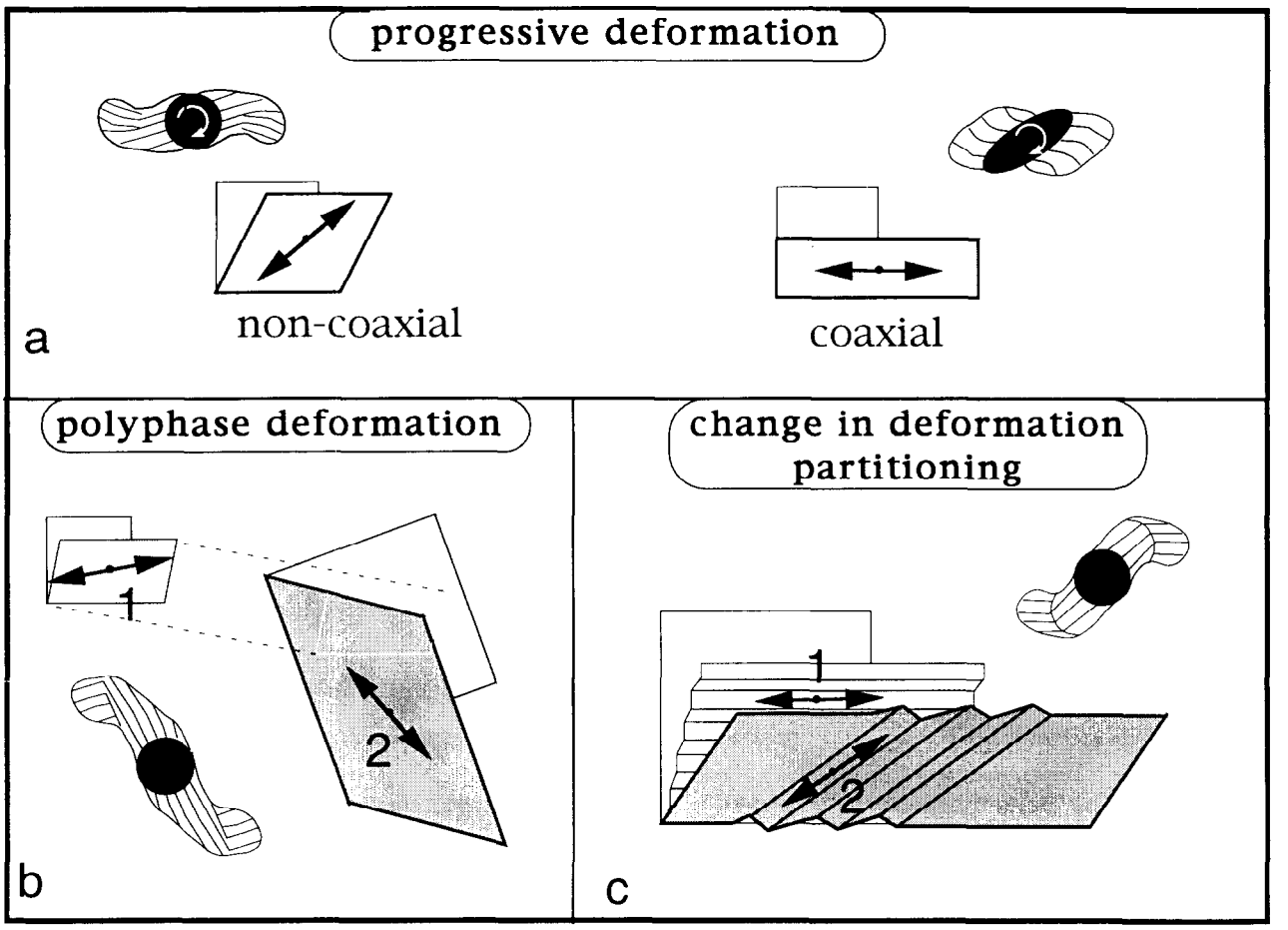

Fig. 8. Possible deformation histories leading to asymmetric pyrite-fringe complexes. Increased shading intensity marks a further advanced kinematic stage. Double arrows mark the orientation of the instantaneous stretching axes (ISA). (a) Non-coaxial and coaxial progressive deformations. (b) Two superimposed deformation phases. (c) Anisotropy-induced repartitioning of the deformation during advanced deformation stages. Deformation is partitioned in domains of non-coaxial and coaxial deformation. Rigid grains are inferred to nucleate domains of coaxial strain around them and undergo foliation-parallel extension which does not coincide with bulk extension directions.

and, as discussed, this can be due to either a polyphase strain path or a change in deformation partitioning (Figs. 8b&c). At Lourdes, a polyphase strain path is recorded by the development of two regional crenulation cleavages which, in the matrix of our pyrite-fringe complexes, are preserved as relics in the strain shadows (Figs. 5 and 9). Their orientations correspond well with the orientation of PCT branches and of individual fibres. Distal (older) fibres and PCT branches are sub-parallel to S_2 whereas proximal (younger) ones are parallel to S_3, consistent with continuous fibre growth during D_2 and D_3.

The kinematic sequences of fringe growth obtained by the present reconstruction can be oriented in the regional tectonic framework, based on the assumption that strain fringes initially developed parallel to S_2 and that S_2 was sub-horizontal (Fig. 11). The latter is justified by the sub-horizontal orientations of D_2 branches in PCTs that have straight D_3 branches (Figs. 10b–d). The latter excludes the D_2 segments having rotated during D_3. In contrast, where the D_3 segment of PCTs are curved (Figs. 10a,e&f), the corresponding D_2 segments are variably inclined to the north, proportional to the curvature angle in the D_3 segment. Thus, it is reasonably assumed that D_2 fringes developed generally in horizontal directions but differentially rotated northward as a function of shape-induced rotations.

Applied to each fringe increment of Figs. 10(a)–(f), the assumption of horizontal D_2 fringes produces a consistent kinematic picture oriented relative to the earth's surface (Figs. 11a–f). Variation in PCT and fringe shapes are logically explained in terms of different initial orientations and shapes of pyrite grains and, consequently, variable mechanical interactions between pyrite and accumulated fringe stages. One can indeed recognize: (1) antithetic slip along a favourably oriented pyrite-fringe interface, which accommodates synthetic spin of the rigid pyrite grains and the fringes (Fig. 11f; Ildefonse & Mancktelow 1993) and (2) pyrite grains being forced to deflect around an obstructing entrant of the D_2 fringe stage (Figs. 11a&e). Both effects contribute to a curved translation direction (PCTs) during D_3. Sharply kinked PCTs with straight branches thus reflect a pyrite-fringe interface geometry that neither favoured antithetic slip nor obstructed pull-apart between the D_2 fringe and the pyrite grain. The variable rotations of pyrite grains are consistent with the different orientations of the (S_1) inclusion trails (Fig. 9). Even opposite rotations are predicted for some grains whose long axes

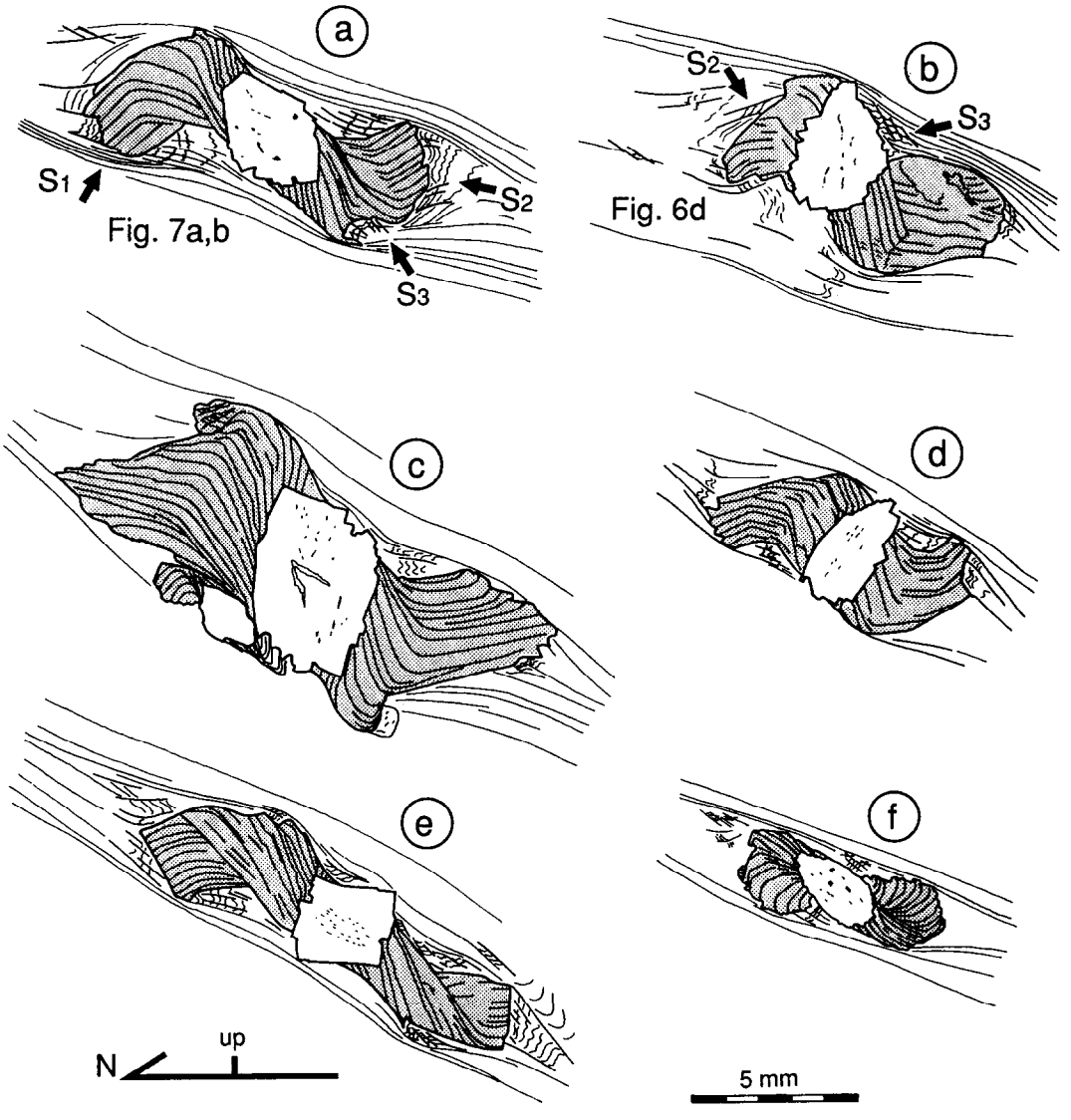

Fig. 9. Microstructural diagrams of six pyrite-fringe complexes representing a wide range of different geometries. All are drawn from N–S trending, vertical thin sections parallel to the stretching lineation. Horizontal and north are indicated by the arrow at the bottom left-hand side. The variable orientation of S_1 inclusion trails inside pyrite grains suggest differential rotations. Relics of two crenulation cleavages are preserved in strain-protected zones associated with the complexes. Some examples shows a particularly sharp change in fibre direction (b). Other specimens (a and f) show smoother fibre curvature.

aligned in a different incremental strain quadrant, for example the specimen of Fig. 11(d) during D_2.

DISCUSSION

Strain fringes as kinematic indicators

The pyrite porphyroblasts from Lourdes clearly rotated relative to the horizontal. In contrast, inclusion-trail data from silicate porphyroblasts suggest that porphyroblasts commonly do not rotate (Bell 1985, Aerden 1995 and references therein). This has been attributed to a particular mechanism of deformation partitioning and the prevalence of pressure-solution processes in metamorphic rocks. The non-rotation of rigid objects requires, however, a coherent object–matrix interface. This is not the case for a pyrite grain developing strain fringes and the rotation of these bodies is, therefore, not contradictory with lack of rotation of porphyroblasts with coherent boundaries.

In fact, the partitioning of deformation around pyrite-fringe complexes as a whole does not differ from that around rigid objects in general. Our PCT analysis showed the pull-apart directions to be parallel to crenulation cleavages, independent of strong variation in local strain parameters (e.g. shear strain) and microstructural development of the matrix. The matrix of the microstructures analysed here lack a crenulation cleavage, except as relics in strain shadows. Yet, the fringes still record S_2 and S_3 parallel pull-apart, highly oblique to the main shearing fabric in the matrix (S_1). This can be attributed to a mechanism of deformation partitioning using two shearing systems: a synthetic system, parallel to a regional crenulation cleavage, and an antithetic system, parallel to the older anistropy (Fig. 13). Where the presence of a rigid object did not allow extension and shearing of the pre-existing foliation in strain shadows,

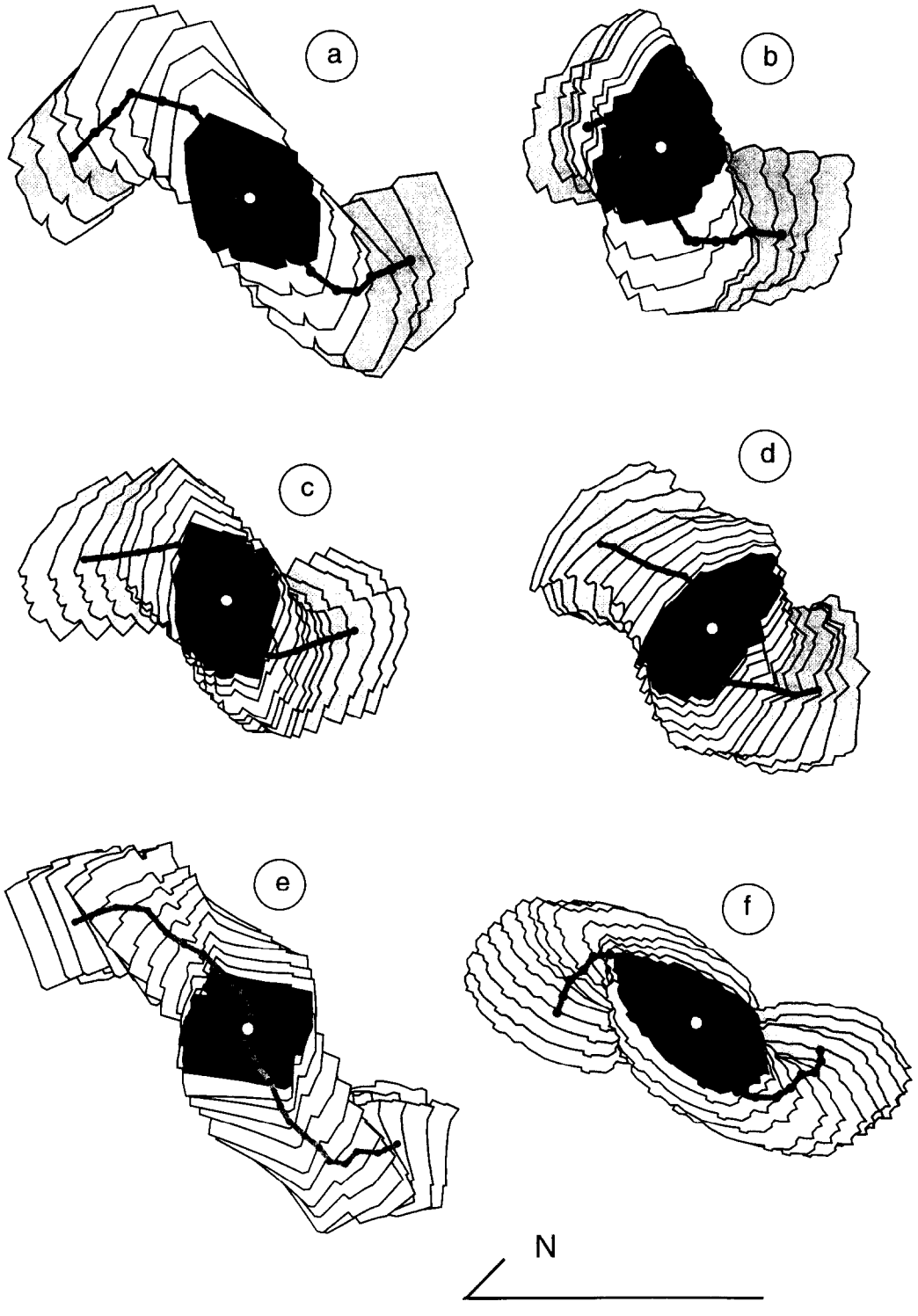

Fig. 10. Reconstruction of the relative displacement path between fringes and pyrite grains by incrementally displacing and rotating a pyrite grain such that the natural fibre pattern is most faithfully reproduced. See text for details of method. Pyrite centre trajectories (PCTs) are hook-shaped and record a sudden change in relative pull-apart direction between pyrite grains and fringes. Labelling corresponds to that in Figs. 9 and 11.

synthetic, S_3 parallel shear strain concentrated against it to accommodate strain and vorticity contrasts with the matrix. This is the same mechanism that permits lack of porphyroblast rotation in zones of intense non-coaxial deformation (Aerden 1995, fig. 11). Rheological heterogeneities, such as pyrite-fringe complexes, veins or silicate porphyroblasts, thus permit recognition of polyphase deformation histories and regional bulk shortening directions in zones where shearing and stretching of pre-existing foliations has destroyed or not allowed development of later cleavages (Fig. 13).

Implications for thrust kinematics

The characteristic asymptotic curvature of foliations towards thrust planes reflects increased horizontal

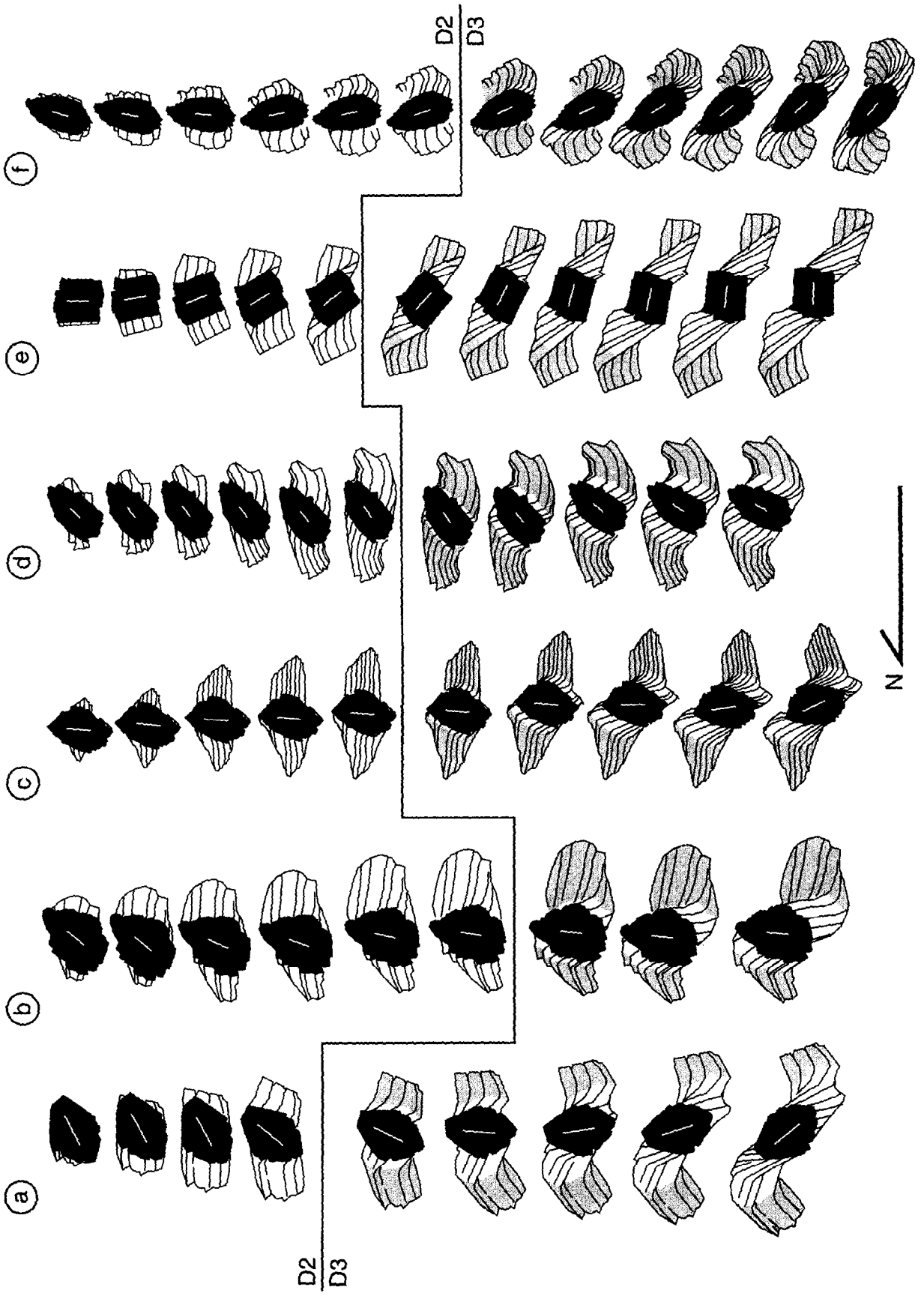

Fig. 11.

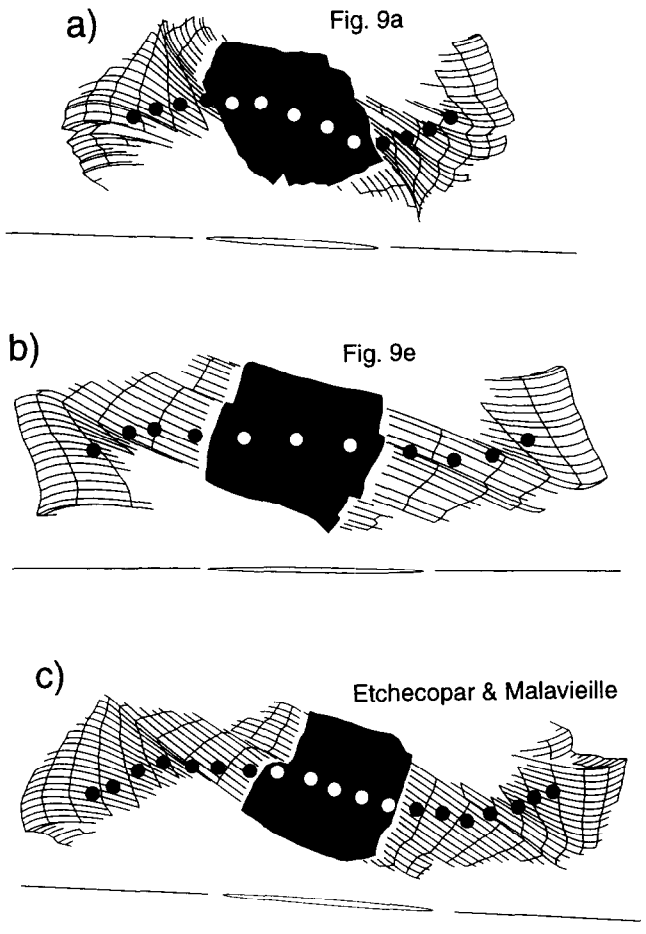

Fig. 12. Numerical modelling of pyrite grains (a) and (e) (Fig. 9) as well as a specimen from Etchecopar & Malavieille (1987, fig. 10), using the computer program they developed. The following features are distinctive: open-ended fibres, not more than 90° fibre curvature and less than 45° curvature of pyrite centre trajectories (PCTs). Near simple shear conditions give best resemblance with the natural homologues.

shearing with depth. Such a shear-strain profile may be superimposed on horizontal (Gray & Willman 1991) or vertical (Elliott 1976) shortening components, depending on the emplacement mechanism of the thrust sheet (compressive or gravitational, respectively). We successfully modelled the S_2 crenulation cleavage and the associated extension fibres to having originated sub-horizontally. This implies sub-vertical shortening components and suggests thrust sheet emplacement by gravitational spreading. The transition from D_2 to D_3 could mark a change from sub-vertical to sub-horizontal shortening in the thrust sheet and a change to a compressive emplacement (assuming that both deformations are syn-thrusting).

However, an alternative explanation for the occurrence of multiple crenulation cleavages in thrust sheets must be considered. The D_2 and D_3 segments of strain fringes could be separated by a (large scale) rigid body rotation that did not contribute to fringe growth. For example, rotation of a thrust sheet as it passes over the upper edge of a thrust ramp could have rotated a steep (compressive) cleavage to a more gently dipping orientation, after which continued deformation caused the rotated cleavage to be overprinted 'by itself'; i.e. by a new crenulation cleavage forming in the original (steep) orientation (Beutner *et al.* 1988).

Thus, two possibilities can be envisaged: (1) an external change in tectonic regime (genuine polyphase deformation) or (2) progressive deformation intermitted by a rigid body rotation. I consider the former mechanism the most realistic and in better agreement with the presented data. Firstly, thrusting at Lourdes involved ductile deformation under greenschist facies conditions, both in hangingwall and footwall units. The thrust represents a ductile shear zone and it is doubtful if the fault-mechanic concept of rigid thrust ramps can be extrapolated to these conditions. Furthermore, the space problem associated with the rotation of a large volume of rock over a ramp is expected to have led to internal pervasive deformations. However, there is no evidence for intermittent deformation between S_2 and S_3 development in the strain fringe record. Finally, bends or ramps in anastomosing ductile shear zones do generally not exceed 45° and generally lie closer to 30°. This is largely insufficient to account for the rigid body rotations of near 90° that would be required to explain the geometry of our PCTs.

In contrast, the alternative explanation of a switch in thrusting mechanism from gravitational spreading, associated with thrust-sheet thinning, followed by a compressive emplacement, associated with thrust-sheet thickening, is consistent with the tectonic history of the area. East–west syn-D_1 extension pre-dates the strain fringes and may be related to Late-Cretaceous transpression parallel to the North Pyrenean Fault (Choukroune 1976, Choukroune & Mattauer 1978) producing a steep foliation (S_1). Early uplift of the Pyrenean chain associated with this transpression probably did not involve large scale thrusting. Plate convergence became less oblique during Eocene times (Choukroune 1976, Choukroune & Mattauer 1978) and caused a build-up of north–south directed compressive forces. The eventual nucleation of thrusts may have been associated with a rapid and permanent drop of horizontal forces within the orogen due to a relatively low shear strength of thrust planes and less effective transmission of plate-tectonic forces. Horizontal forces had been supporting a high relief and thick crust and their sudden decrease could explain gravitational instability and partial col-

Fig. 11. Kinematic development of different pyrite–fringe complexes oriented relative to the horizontal (north is to the left). The D_2 segments of pyrite fringes are assumed to have developed parallel to a sub-horizontal S_2. (a)–(f) correspond to the same letters in Figs. 9 and 10; D_2 and D_3 development stages are separated by a continuous line. Differential rotations between different pyrite grains are predicted. Differences in PCTs can be observed to result from variable interaction between the rigid pyrite grain and its progressive fringe stages, particularly with the D_2 fringe segment (shaded) during D_3 deformation. Note the opposite rotation of specimen (d) during D_2, consistent with its particular initial orientation in a D_2 flow with sub-vertical shortening component.

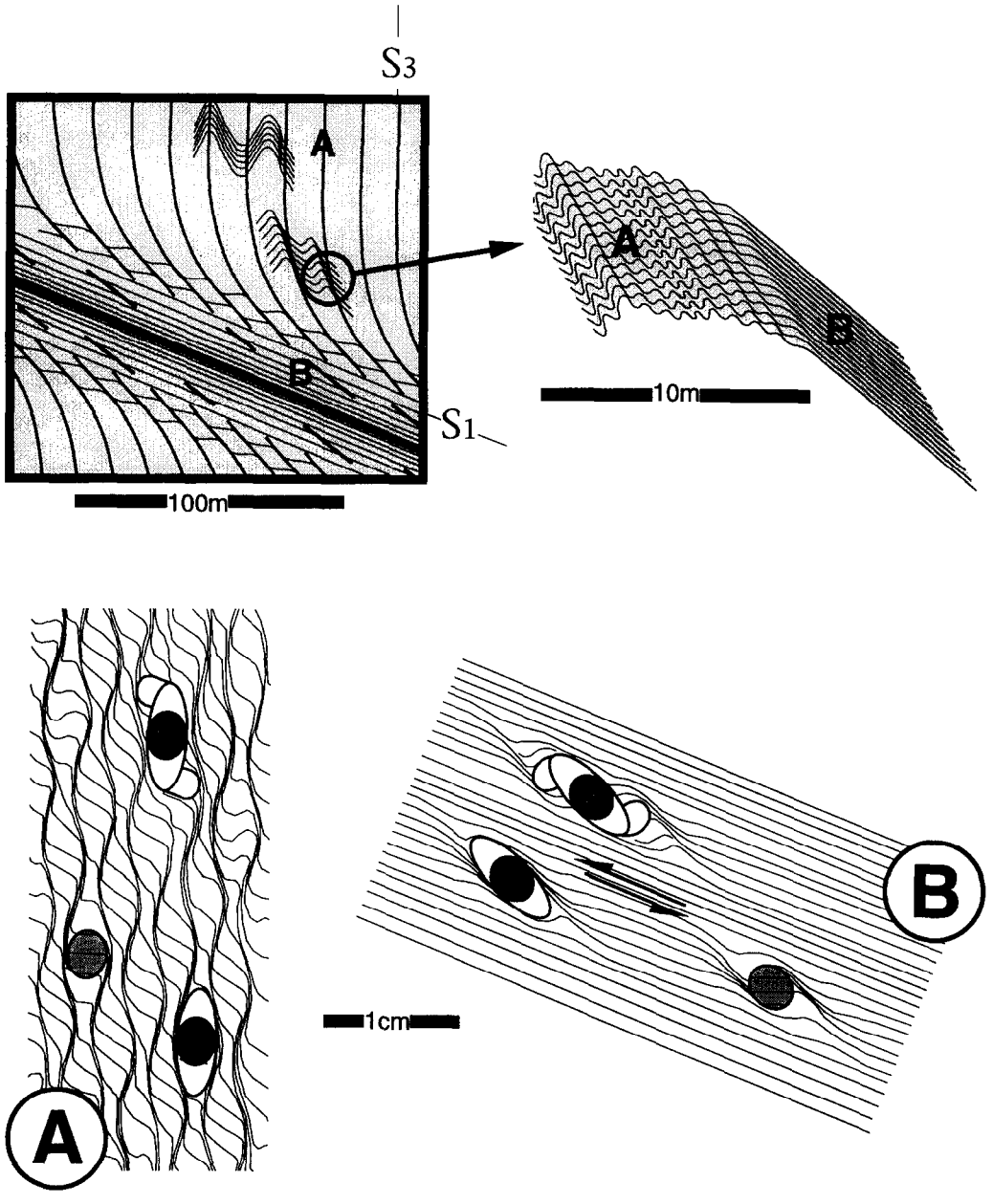

Fig. 13. Conceptual relationships between end-member microstructural developments (a & b) and position in the heterogeneous strain field of the study area. A hypothetical silicate porphyroblast is drawn with coherent boundaries (shaded) and two pyrite porphyroblasts with different timing (black). The older one records both D_3 and D_2 strain in a hooked strain fringe. The partitioning of deformation is controlled by two shearing systems, a synthetic one parallel to the new crenulation cleavage and an antithetic one parallel to the pre-existing main foliation S_1. Zones with relatively coaxial or low strain are dominated by crenulation cleavage development (a). In zones where the pre-existing foliation has an extensional orientation (b), crenulations are absent and the only evidence for a polyphase deformation history is provided by rigid objects against which synthetic shear-strain bands nucleated and whose strain shadows may contain relic crenulations. The strain diagram (a) and (b) show coarse-scale partitioning features. Finer-scale strain partitioning superimposed on them accounts for a closer spacing of crenulations in (a) and the presence of relic crenulations in the strain shadow regions of (b).

lapse (D_2) of the orogen (Fig. 14). Renewed compression (horizontal shortening) during D_3 indicates recovered gravitational equilibrium, perhaps by a combination of factors such as rapid denudation (lowered relief), forward propagation of thrusts (lowering of the orogen taper) and thermal re-equilibration (increased viscosity). Both the D_2 and D_3 events involved stretching in north–south cross-sections and explain the north–south lineation induced on the dominant foliation S_1. The weak, sub-horizontal S_4 cleavage found in the southern part of the study area may reflect a second collapse episode of minor importance, due to ceasing plate convergence.

Comparison with previous methods

The most commonly used method to reconstruct strain paths from displacement-controlled strain fringes was introduced by Durney & Ramsay (1973) and later modified by Ramsay & Huber (1983) and Beutner & Diegel (1985). Fibres are decomposed in line segments that are considered to track incremental extension direc-

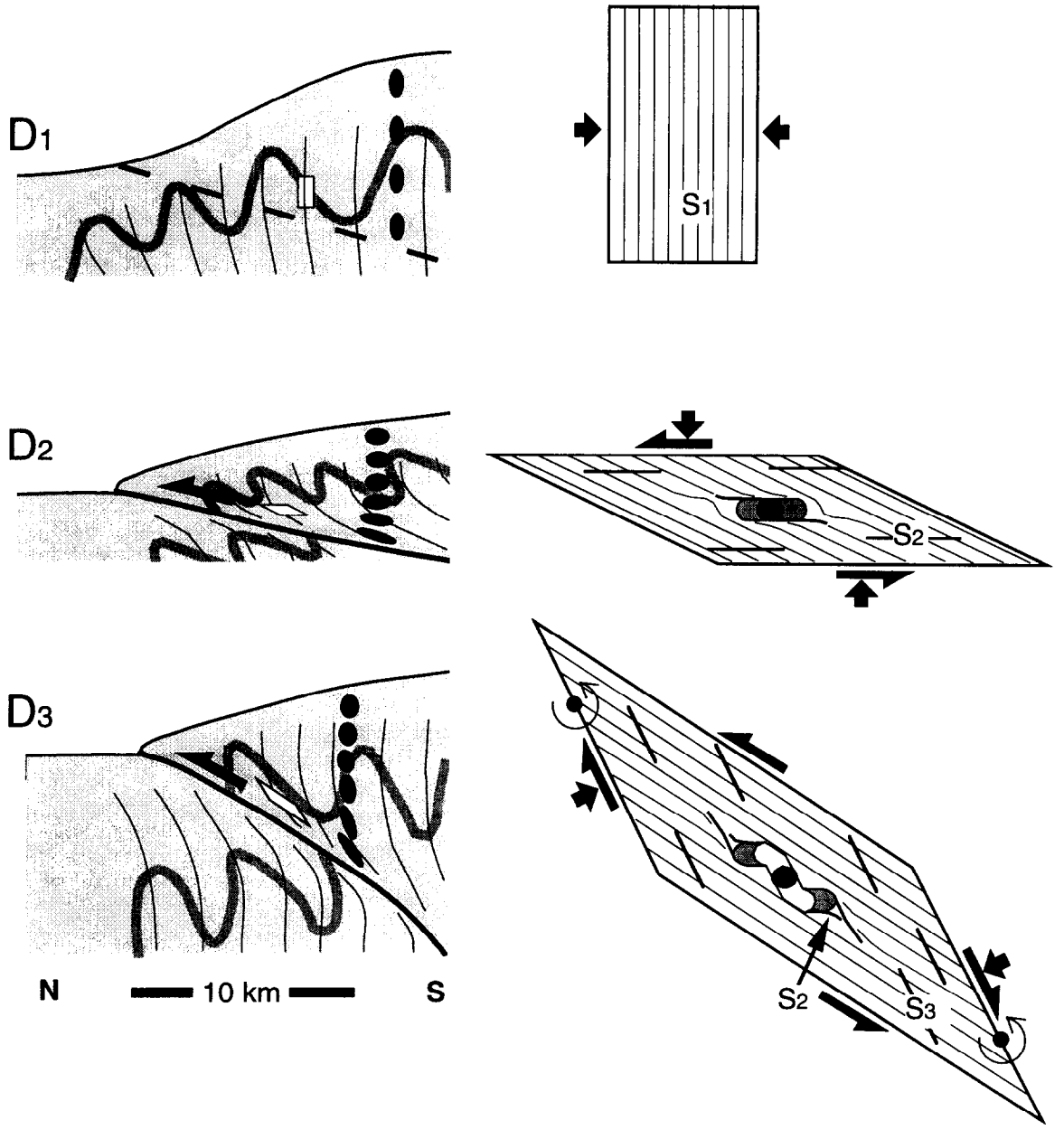

Fig. 14. Tectonic model showing possible relationship between the kinematics of pyrite-fringe complexes, foliation development and thrusting. Black strain ellipses do not illustrate finite strain but the geometry of each deformation phase. During D_1, a steep foliation is generated during sinistral transpression parallel to the North Pyrenean fault. Less oblique plate convergence produces thrusts during D_2 and this triggers gravitational collapse of the previously uplifted Pyrenean orogen due to less effectively transmitted tectonic forces. The thrust sheet undergoes thinning as it is emplaced by gravitational spreading. A sub-horizontal crenulation cleavage is generated and early syn-D_2 pyrites develop strain fringes. After gravitational equilibrium has been recovered (see text for possible factors), horizontal tectonic forces dominate and generate a new steep crenulation cleavage (S_3) related to crustal thickening. Strain fringes now develop in a steep direction.

tions around the pyrite grains. Ramsay & Huber (1983) originally applied their method in the X–Y plane of deformation (in the cleavage plane). In this plane, progressive deformation is coaxial and pyrite grains do not rotate. Therefore, all fibre curvature must be due to changes in bulk strain parameters, either reflecting a polyphase deformation history or gradual rotations of bulk shortening directions, such as inferred by Durney & Ramsay (1973) from curved fibres in the Helvetic Alps, where they correlated the fibre directions with changes in (gravitational) nappe transport directions.

However, the same method used in the X–Z plane of non-coaxial deformations (Beutner & Diegel 1985, Fischer & Byrne 1992, Fisher & Anastasio 1994) requires caution, as fibre curvature will now only track pull-apart directions if the rigid object and the fringes did not rotate relative to the plane of shearing. Only in that situation would fibres be determined entirely by

translations and track the cumulative strain ellipse. Beutner & Diegel (1985) already admitted this as an uncertainty factor and therefore restricted use of the technique to spherical framboidal pyrites. This study shows that such rigid body rotations are actually determinant for fibre curvature (at least for angular grains) and that Durney & Ramsay's method yields the incorrect shear sense at Lourdes. Furthermore, Seegers (1992) analysed perfectly spherical pyrite framboids with 'pyrite-type' quartz fringes from the Yilgarn Craton, Australia and he concluded that these bodies had also rotated relative to the plane of shearing. I have applied my method to one of his specimens (courtesy of C. Passchier) and this also predicted that the grains rotated. It actually showed a hooked PCT, very similar to the ones obtained at Lourdes, suggesting two deformation phases (Aerden, unpublished data). Durney & Ramsay's method and later modifications must, therefore, be considered unreliable for the X–Z plane.

Ellis' method applies only to the relatively rare combination of spherical pyrite grains with deformable antitaxial fibres. He considered that strain fringes and angular pyrite grains both rotate in non-coaxial deformations, but that spherical pyrite grains do not, because he speculated that friction between the matrix and the pyrite grain would be too low for a shear couple to build up. As already pointed out, this is a doubtful assumption.

Etchecopar and Malavieille (1987) have taken a completely different approach, based on minimization of the area overlap between incremental pyrite-fringe complex stages and the deforming matrix. Their method incorporates both rotations and translations between fringes and pyrite grains. In contrast to previous methods, now the rotations determine the fibre curvature sense and this gives the correct shear sense at Lourdes. Nevertheless, the method is limited by a lack of geometrical and rheological constraints. The matrix foliation is modelled as a mechanically passive, non-material plane instead of a plane of deformation partitioning (Bell 1985). Consequently, matrix is allowed to partially fill the incremental space created at the pyrite-fringe interface, resulting in open-ended fibres, not in contact with the pyrite grain (Fig. 12).

A shortcoming of all the previous methods is that none clearly distinguishes between progressive deformations and polyphase deformations. Polyphase deformation has been sometimes inferred from certain matrix microstructures and fibre geometries, but the advantage of the present method is that it constrains a single- or polyphase strain directly from the strain fringe geometry, even where such a history is not immediately evident from matrix microstructures. Furthermore, all previous methods assume that pull-apart directions around pyrite grains track the bulk accumulative strain ellipse of the matrix and therefore rotate towards the shear plane. This study shows that pull-apart between pyrite grains and their fringes may be relatively coaxial parallel to a crenulation cleavage, even if bulk strain is non-coaxial. This is explained by shear strain concentration in the crenulation cleavage planes, which anastomose around coaxial strain microlithons containing the rigid objects (Fig. 13).

CONCLUSIONS

(1) Fibre curvature in displacement-controlled strain fringes result from the opposed effects of (i) rotation of the pull-apart direction between fringes and the rigid object and (ii) shape-induced rotations of both the rigid object and its fringes. The second factor largely determines the curvature sense and asymmetry of strain fringes.

(2) Strongly sigmoidal strain fringes with high-angle internal truncation surfaces indicate a polyphase deformation history and can provide both the local shear sense as well as bulk shortening directions for multiple deformations. As such, they are valuable kinematic tools in tectonic studies.

(3) At Lourdes, strain fringes record a two-phase deformation history, comprising a transition from subhorizontal to sub-vertical extension in a thrust sheet, superimposed on a northward shearing. This is tentatively interpreted in terms of gravitational spreading, followed by a compressive emplacement.

Acknowledgements—I thank J. Malavieille for a joint field trip to the study area during which we located key outcrops. F. Niño for assistance with the Etchecopar & Malavieille (1987) computer program and C. Passchier for discussion and for allowing study of his collection of spherical pyrite-fringe complexes from the Yilgarn craton. Thoughtful reviews by E. Beutner and an anonymous reviewer were greatly appreciated and led to considerable improvements. This investigation was supported by a Human Capital and Mobility post-doctoral Fellowship from the European Commission to the author (Contract No. ERBCHBICT930263).

REFERENCES

Aerden, D. G. A. M. 1995. Prophyroblast non-rotation during crustal extension in the Variscan Pyrenees. *J. Struct. Geol.* **17**, 709–726.

Bell, T. H. 1985. Deformation partitioning and porphyroblast rotation in metamorphic rocks: a radical reinterpretation. *J. Metamorph. Geol.* **3**, 109–118.

Bell, T. H. 1986. Foliation development and refraction in metamorphic rocks: reactivation of earlier foliations and decrenulations due to shifting patterns of deformation partitioning. *J. Metamorph. Geol.* **4**, 421–444.

Beutner, E. C. & Diegel, F. A. 1985. Determination of fold kinematics from syntectonic fibres in pressure shadows, Martinsburg Slate, New Jersey, *Am. J. Sci.* **285**, 16–55.

Beutner, E. C., Fischer, D. M. & Kirkpatrick, J. L. 1988. Kinematics of deformation at a thrust ramp (?) from syntectonic fibers in pressure shadows. *Spec. Pap. Geol. Soc. Am.* **222**, 77–88.

Choukroune, P. 1969. Sur la Présence, le style et l'age des tectoniques superposées dans le Crétacé nord-Pyrénéen de la région de Lourdes (Hautes-Pyrénées). *Bull. B.R.G.M.* (2), Section I **2**, 11–20.

Choukroune, P. 1971. Contribution à l'étude des mécanismes de la déformation avec schistosité grâce aux crisytallisations syncinématiques dans les 'zones abritées' ('pressure shadows'). *Bull. Soc. géol. Fr.* **13**, 275–271.

Choukroune, P. 1976. Strain patterns in the Pyrenean Chain. *Phil. Trans. R. Soc. Lond.* **A283**, 271–280.

Choukroune, P. & Mattauer, M. 1978. Tectonique des plaques et Pyrénées: sur le fonctionnement de la faille transformante nord-pyrénéenne; comparaisons avec des modeles actuels. *Bull. Soc. géol. Fr.* **20**, 689–700.

Choukroune, P., Mattauer, M. & Rios, L. M. 1980. Estructura de los Pirineos. *Bol. geol. Min.* T, **XCI-I**, 213–248.

Dietrich, D. 1989. Fold-axis parallel extension in an arcuate fold- and thrust-belt: the case of the Helvetic Nappes. *Tectonophysics* **170**, 183–212.

Durney, D. W. & Ramsay, J. G. 1973. Incremental strains measured by syntectonic crystal growths. In *Gravity and Tectonics* (edited by DeJong, K. A. & Scholten, R.) Wiley, New York, 67–95.

Elliott, D. 1976. The energy balance and deformation mechanisms of thrust sheets. *Phil. Trans. R. Soc. Lond.* **A283**, 289–312.

Ellis, M. A. 1986. The determination of progressive deformation histories from antitaxial syntectonic crystal fibres. *J. Struct. Geol.* **8**, 701–709.

Etchecopar, A. & Malavieille, J. 1987. Computer models of pressure shadows: a method for strain measurement and shear-sense determination. *J. Struct. Geol.* **9**, 667–677.

Fischer, D. & Bryne, T. 1992. Strain variations in an ancient accretionary complex: implications for forearc evolution. *Tectonics* **11**, 330–347.

Fisher, D. & Anastasio, D. J. 1994. Kinematic analysis of a large-scale leading edge fold, Lost River Range, Idaho. *J. Struct. Geol.* **16**, 337–354.

Gray, D. R. & Williams, C. E. 1991. Thrust-related strain gradients and thrusting mechanisms in a chevron-folded sequence, southeastern Australia. *J. Struct. Geol.* **13**, 691–710.

Hanmer, S. K. & Passchier, C. W. 1991. Shear sense indicators: a review. Geological Survey of Canada, Ottawa, Paper 90-17, 72 pp.

Ildefonse, B. & Mancktelow, N. S. 1993. Deformation around rigid particles: the influence of slip at the particle/matrix interface. *Tectonophysics* **221**, 345–359.

Kirkwood, D., Malo, M., St-Julien, P. & Therrien, P. 1995. Vertical and fold-axis parallel extension within a slate belt in a transpressive setting, northern Appalachians. *J. Struct. Geol.* **17**, 329–344.

Müggе, O. 1930. Bewegungen von porphyroblasten in phylliten und ihre messung. *Neues Miner. Geol. Palaoent.* **61**, 469–520.

Pabst, A. 1931. 'Pressure shadows' and the measurement of the orientations of minerals. *Am. Miner.* **16**, 55–61.

Passchier, C. W. & Trouw, R. A. J. 1995. *Microtectonics*. Springer, Heidelberg, 300 pp.

Ramsay, J. G. 1980. The crack–seal mechanism of rock deformation. *Nature* **284**, 135–139.

Ramsay, J. G. & Huber, M. I. 1983. *The Techniques of Modern Structural Geology, Volume* 1: *Strain Analysis*. Academic Press, London.

Seegers, P. 1992. Syntectonic tracking and non-tracking fibres in pressure fringes from the Leonora region, Yilgarn Craton, Australia. Unpublished M.Sc. thesis, Utrecht).

Spencer, S. 1991. The use of syntectonic fibres to determine strain estimates and deformation paths: an appraisal. *Tectonophysics* **194**, 13–34.

Spry, A. J. 1969. *Metamorphic Textures*. Pergamon Press, Oxford.

Wickham, J. S. 1973. An estimate of strain increments in a naturally deformed carbonate rock. *Am. J. Sci.* **273**, 23–47.

Wickham, J. & Anthony, M. 1977. Strain paths and folding of carbonate rocks near Blue Ridge, central Appalachians. *Geol. Soc. Am. Bull.* **88**, 920–924.

Zwart, H. J. & Oele, J. A. 1966. Rotated magnetite crystals from the Rocroi Massif (Ardennes). *Geol. Mijnb.* **45**, 70–74.